Solid Freeform Fabrication 2017: Proceedings of the 28th Annual International Solid Freeform Fabrication Symposium – An Additive Manufacturing Conference
Reviewed Paper

EFFECT OF SPECIMEN SURFACE AREA SIZE ON FATIGUE STRENGTH OF ADDITIVELY MANUFACTURED TI-6AL-4V PARTS

Jonathan Pegues[1], Michael Roach[2], R. Scott Williamson[2], Nima Shamsaei[1,*]

[1]*Laboratory for Fatigue & Additive Manufacturing Excellence, Department of Mechanical Engineering, Auburn University, Auburn, AL 36849*

[2]*Department of Biomedical Materials Science, University of Mississippi Medical Center, Jackson, MS 39216*

[*]Corresponding author: shamsaei@auburn.edu

Abstract

As additive manufacturing becomes an increasingly popular method for advanced manufacturing of components, there are many questions that need to be answered before these parts can be implemented for structural purposes. One of the most common concerns with additively manufactured parts is the reliability when subjected to cyclic loadings which has been shown to be highly sensitive to defects such as pores and lack of fusion between layers. It stands to reason that larger parts will inherently have more defects than smaller parts which may result in some sensitivity to surface area differences between these parts. In this research, Ti-6Al-4V specimens with various sizes were produced via a laser-based powder bed fusion method. Uniaxial fatigue tests based on ASTM standards were conducted to generate fatigue-life curves for comparison. Fractography on the fractured specimens was performed to distinguish failure mechanisms between specimen sets with different sizes.

Keywords: Fatigue; Additive manufacturing; Surface effects; Microstructure; Titanium alloys

Introduction

Additive manufacturing (AM) of components has become an increasingly popular advanced manufacturing process in many industries. In the biomedical industry the AM process offers customized implants that can be directly tailored to an individual. Titanium alloys such as Ti-6Al-4V are widely used in biomedical applications due to their excellent biocompatibility [1 - 4]. Traditionally these implants have been produced via subtractive manufacturing from wrought materials in which extensive research into the durability under various conditions has been conducted [4 – 10]. One of the biggest challenges AM produced materials must overcome before being fully implemented into structural and biomedical applications is the uncertainty of the fatigue behavior compared to traditional wrought alloys [11]. Research has shown that the fatigue life of AM parts shows a reduction in fatigue limits which is even greater for as-built parts that don't undergo post-process machining to remove the rough surface [12 – 14]. While much improvement in the additive process has been achieved in recent years, there is still a need to better understand the fatigue behavior of AM parts before they are fully implemented into structural applications.

AM parts have shown high sensitivity to defects inherent to the AM process such as voids and lack of fusion (LoF) between layers [14 – 16]. LoF between layers typically results in seemingly fully dense parts, however, these "pancake like" voids contain little volume yet create high stress concentrations along the edges. As such, the LoF areas are prime crack initiation sites which contribute to the reduced the fatigue life observed in AM parts. Additionally, for as-built parts, the effect of surface area may prove to be detrimental to the fatigue limit due to roughness induced crack initiation along the surface. Parts that contain similar volume with varying surface areas may result in noticeably different fatigue lives for similar stress amplitudes and thus lower fatigue limits. This research specifically addresses the issue of increasing surface area for AM parts produced via a laser-based powder bed fusion (L-PBF) method through the use of several microscopic techniques.

Materials and Methods

Three sets of specimens were designed to produce increasing gage surface area while maintaining a constant gage volume of approximately 123 mm^3. The chosen specimen geometries are shown in Figure 1 along with the calculated surface area for each specimen type. Specimens were fabricated using a powder bed based EOS M290 with a maximum laser power of 400W. The spherical Ti-6Al-4V alloy powder was supplied with a powder size greater than 15 μm and less than 45 μm. All specimens were built at an angle of 45° from the titanium substrate. Before removal, the specimens were stress relieved to alleviate any residual stress as result of the extreme cooling rates associated with the L-PBF AM process. The stress relief was conducted at 700° C for 1 hr under an Ar environment and allowed to air cool after which the samples were carefully removed from the substrate.

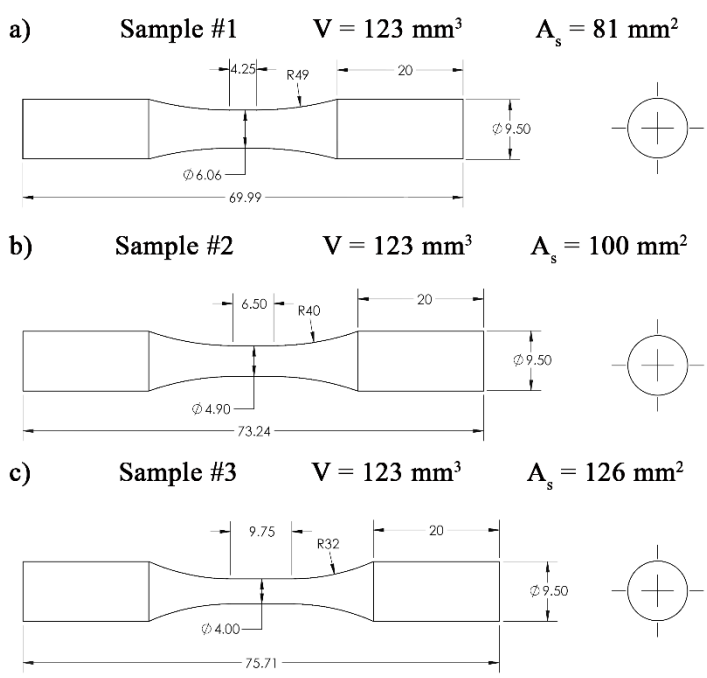

Figure 1: Sample dimensions. All measurements are in mm.

A representative sample was sectioned to determine the as-built microstructure. The microstructure was revealed using Kroll's reagent to etch the polished surface which was then observed using an optical microscope. Further microstructural analysis was performed using scanning electron microscopy (SEM) and electron backscatter diffraction (EBSD) analysis to determine the present phases and grain size. Fatigue tests were conducted on an MTS testing frame with a load capacity of 100 kN. An extensometer was used to record the stabilized hysteresis response for each test then removed so that the samples could be run until failure. Three stress levels were selected to produce a range of fatigue lives from 10^4 cycles and greater than 10^6 cycles. At least two and up to four samples were tested at each stress level for all sample geometries to construct a stress-life (S-N) curve for comparison between the sample types. All tests were run until failure except for tests that exceeded 10^6 cycles which were removed and considered to be runouts. Fractured surfaces were subsequently removed and observed by SEM to identify failure mechanisms related to each specimen.

Experimental Results

Microstructure

The microstructure consisted of mostly acicular α' grains formed as a result of diffusionless phase transformation from the β phase with a small distribution of lath like α phase. This β → α' phase transformation is a result of the extraordinarily high cooling rates associated with the L-PBF process and results in a fully α' + α phase distribution [17, 18]. The microstructure developed in an epitaxial manner resulting in elongated prior β grains oriented parallel to the build direction as shown in Figure 2. The top surface in relation to the build plate had a visually smoother surface compared to the bottom surface as indicated in Figure 2.

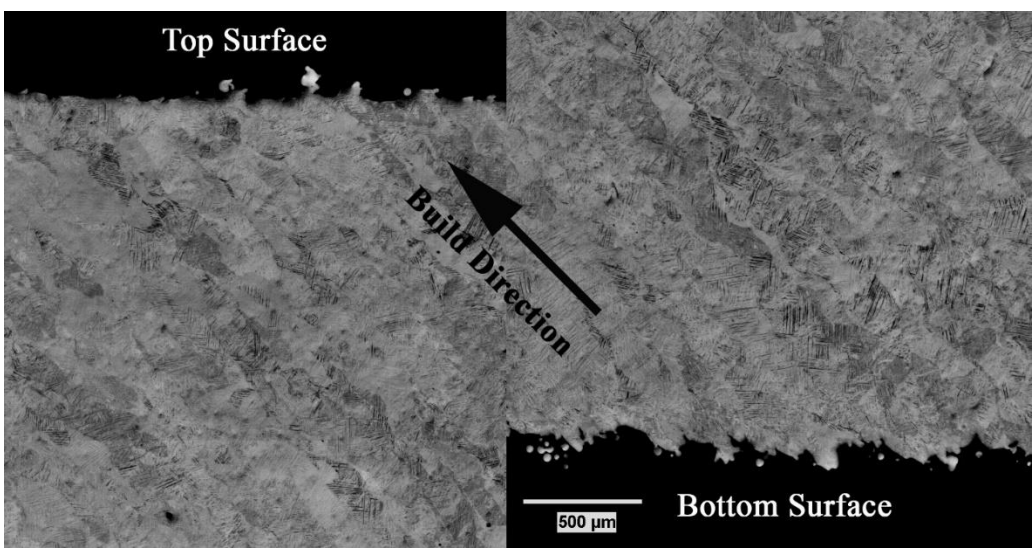

Figure 2: Optical image taken at 50x in the transverse direction. The left side shows upper most portion of the build while the right side shows the bottom most portion.

The microstructure and phase distribution were revealed using EBSD. A representative sample from the transverse direction is shown in Figure 3. The α and α' phases are both hexagonally close packed (HCP) phases and are therefore indistinguishable from each other in the phase map as shown in Figure 3(b). However, the acicular needle like α' phase is visually distinguishable from the lath like α phase within the prior β grains which is shown by the dotted line in Figure 3(a). The phase map does show that the β phase was completely transformed to the α or α' phases upon cooling. Grain size analysis showed similar grain size and shape for the α and α' phases in both the longitudinal and transverse direction which is given in Figure 3(c) and (d) respectively. The average width of the α' grains was approximately 1.5 μm with an average aspect ratio of 0.55.

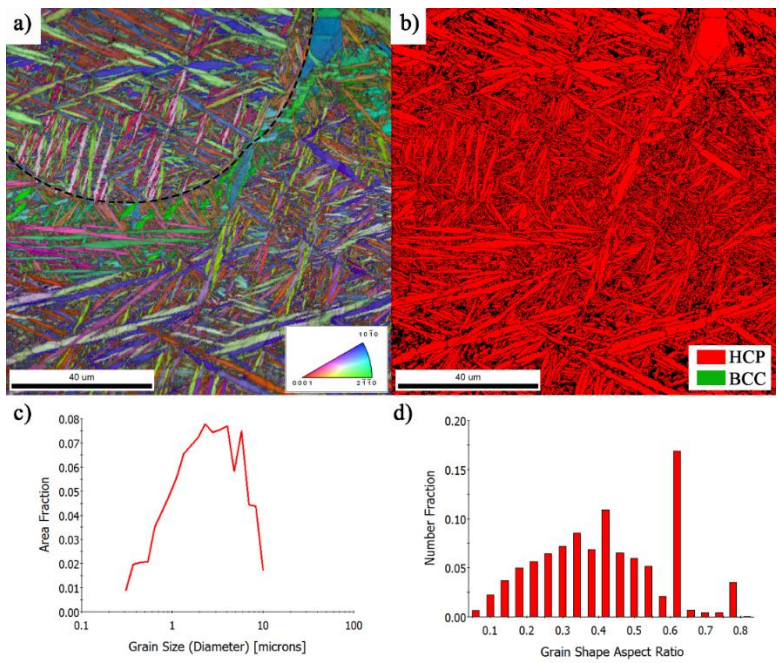

Figure 3: Microstructure of the as-built microstructure showing a) orientation b) phase distribution c) grain size and d) aspect ratio of the grains.

Fatigue Behavior

The S-N behavior of wrought Ti-6Al-4V has been well studied and has been shown to have a fatigue limit in the range of 550 - 750 MPa [19]. For additively manufactured Ti-6Al-4V, however, the fatigue limit has been shown to be significantly reduced, especially for the as-built condition [14]. Fatigue tests were started at a stress amplitude of 450 MPa to establish a sufficient set of stress levels to produce fatigue lives in the desired range. The stress amplitude of 450 MPa produced relatively low cycle fatigue lives (< 20,000 cycles) which is in stark contrast to the fatigue limit of wrought Ti-6Al-4V alloys. It was found that a stress level of 100 MPa was sufficient in producing fatigue lives greater than 10^6 cycles which for this investigation was considered to be approaching the fatigue limit. From these results the stress levels selected to

construct S-N curves for the given geometries were 300 MPa, 200 MPa, and 100 MPa. At least one test for each sample set was conducted at 450 MPa, however, they were not included in the cyclic deformation analysis due to the inconsistent deformation behavior for low cycle fatigue under load controlled conditions.

Cyclic data from the fatigue tests showed that all stress levels resulted in fully elastic deformation as would be expected for Ti-6Al-4V under such low stress amplitudes. Figure 4 shows the hysteresis loops for samples #1 and #3 and show fully elastic deformation for both samples at 300 MPa. All sample geometries resulted in similar cyclic behavior for each stress amplitude and show almost no macroscopic plastic deformation.

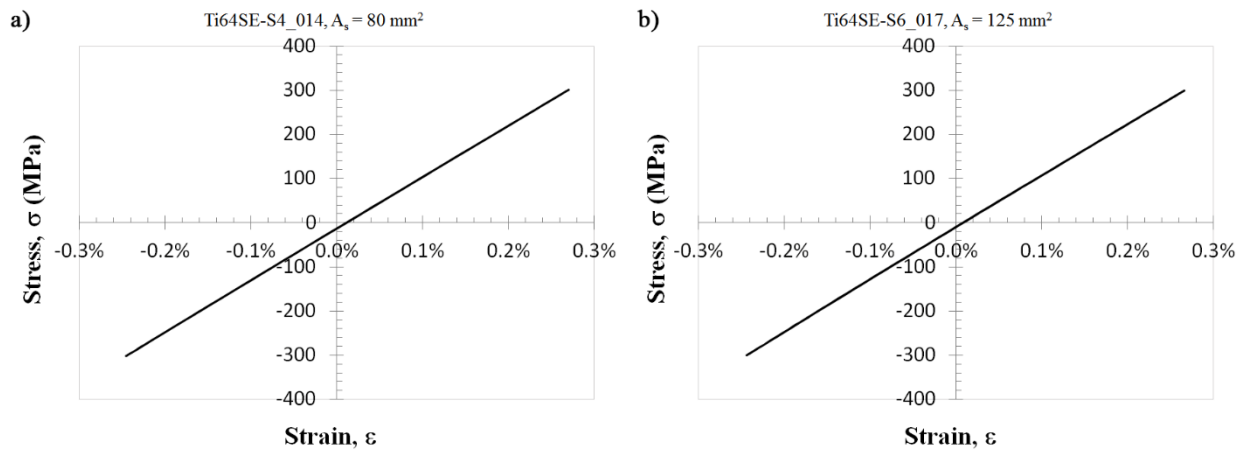

Figure 4: Hysteresis loops for a) sample set #1 and b) sample set #3.

The S-N curve for each sample geometry is given in Figure 5 and shows a clear separation in the stress life of the respective geometries. The arrow in Figure 5 represents tests that were removed once sufficiently past 10^6 cycles without failure. Sample geometries with increased surface area showed a general reduction in fatigue lives at all stress levels at which failure occurred. For the intermediate fatigue lives at a stress amplitude of 200 MPa there is some overlap in the fatigue life ranges between each sample set. However, it can be reasoned that there is an observable reduction of fatigue life for this stress level when considering the average fatigue life for each geometry. For stress amplitudes over 200 MPa the separation in fatigue lives is much clearer for each geometry without overlap between the respective fatigue life ranges. Additionally, the low cycle fatigue lives at 450 MPa are shown in Figure 5. While these tests contain high uncertainty due to the low cycle fatigue behavior for tests in load control conditions, there is an obvious separation in fatigue life at this stress level as well.

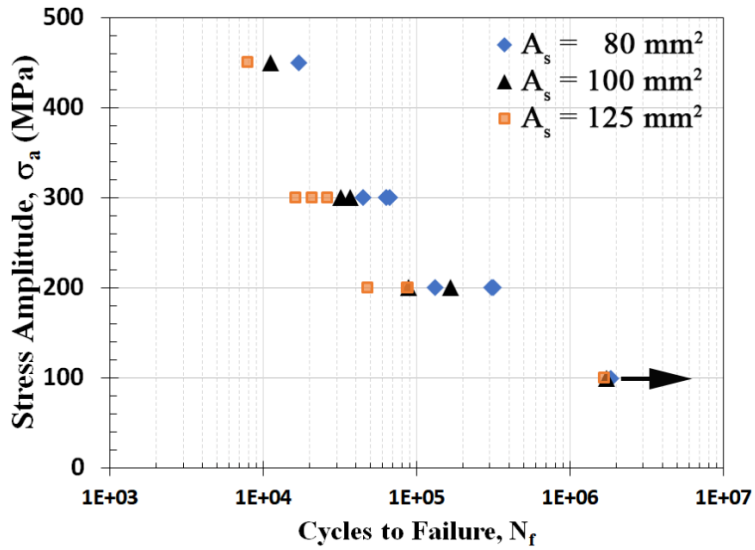

Figure 5: Stress-life curves for each sample geometry.

Fractography

Fractography showed that the fracture surfaces were somewhat similar across all sample geometries in that there were three distinct crack growth zones associated with the fracture surfaces. These zones are shown in Figure 6 where the arrows indicate the crack growth directions.

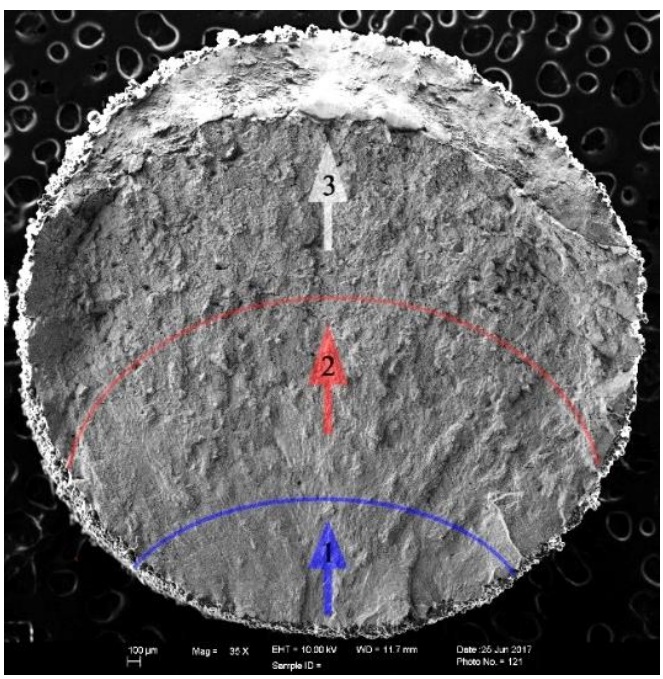

Figure 6: Representative crack growth zones for tested samples.

Interestingly, all cracks initiated on the side that was facing the build plate during fabrication indicating that AM parts in the as-built condition are highly sensitive to build orientation and specifically to any surfaces oriented towards the build plate. Cracks initiated at the surface and almost exclusively at a point where two powder particles were melted together as shown in Figure 7. The arrows in Figure 7 indicate the initiation sites where two powder particles are melted together creating a micro-notch in the already highly rough surface. A tear ridge is formed at the right most initiation site and extends upwards which indicates a change in grain orientations across the tear ridge, possibly a prior β boundary. The crack initially propagates in stage I crack growth mode along crystallographic planes as indicated by the highlighted (red) facets. These facets resemble the martensitic α' needles that were revealed during the microstructure analysis. This initial type of crack growth leads to a relatively tortuous crack path as the crack tends to change directions when encountering discontinuities such as grain boundaries.

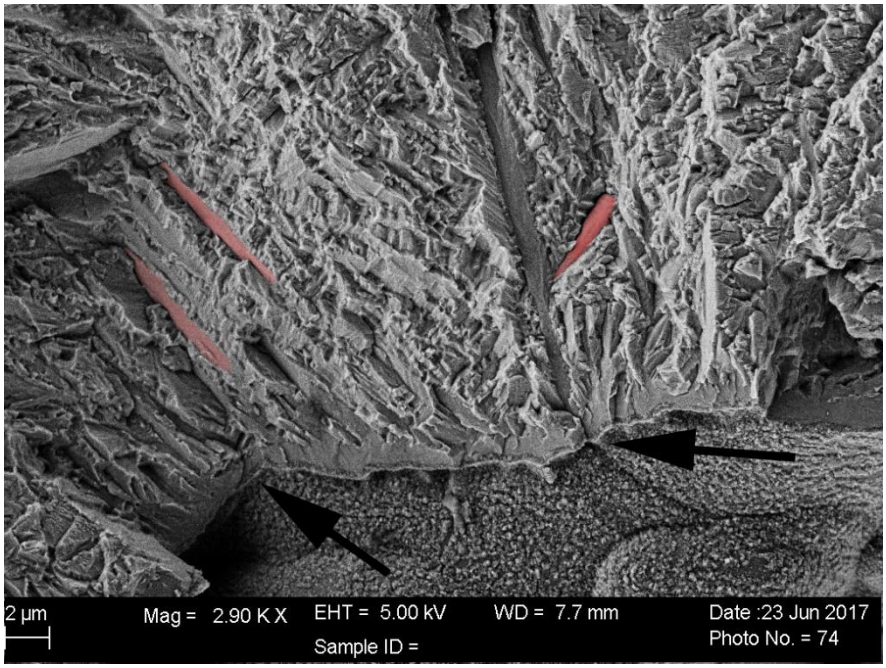

Figure 7: Crack initiation site at joining powder particles (arrows) showing stage one crack growth exposing α' facets (red).

As the crack propagated, a mixture of transgranular and intergranular crack growth along with large secondary cracking and fatigue striations perpendicular to the crack growth direction were observed. Figure 8 gives a representation of these characteristics which were representative of the secondary crack growth zone shown in red in Figure 6. The exposed grain in the center of Figure 8 shows quasi-cleavage characteristics in which an apparent crystallographic plane ruptured while leaving tear dimples across the surface. To the right of the grain in Figure 8, fatigue striations are visible showing the crack front was propagating towards the top left of the image. These features indicate that this secondary zone of crack propagation is a mixture of static failure modes such as cleavage and ductile rupture as well as typical stage II fatigue crack growth with stable striation marks. This combination of failure modes leads to an even more tortuous crack path than the first crack growth zone which is readily observable in Figure 6. The combination of static and

cyclic failure modes could explain the drastically reduced fatigue limit for the L-PBF produced Ti-6AL-4V parts.

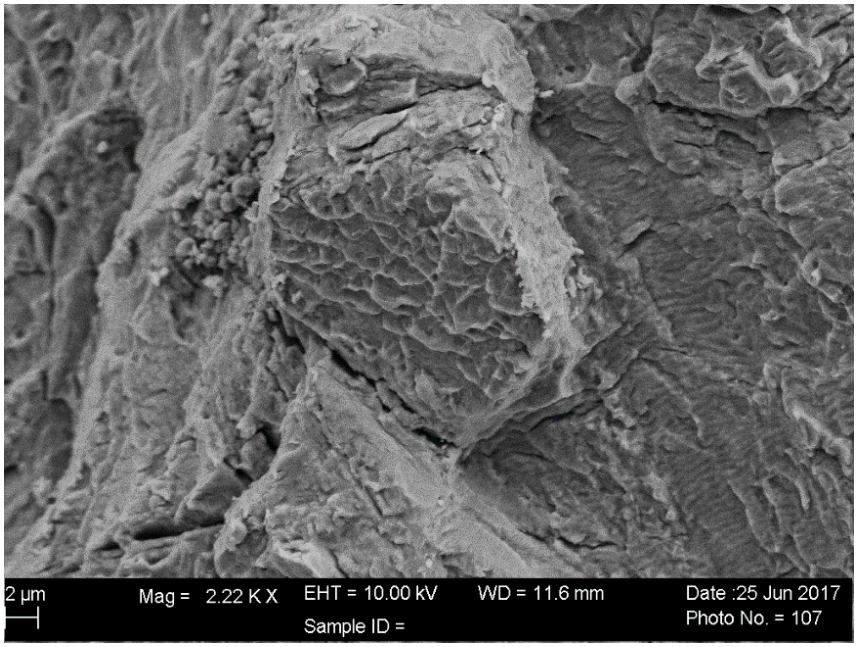

Figure 8: SEM image of the second crack growth zone associated with the AM produced parts.

The final crack growth zone is characterized by severe overload as a result of the decreasing load bearing cross-section from the extending crack. At this stage the part fails in a ductile overload manner. Figure 9 gives a representation of the fracture surface at this stage. The dimple rupture is indicative of micro-void coalescence until the remaining part fails in shear mode as shown by the steep surface along the back ridge of the specimen in Figure 6.

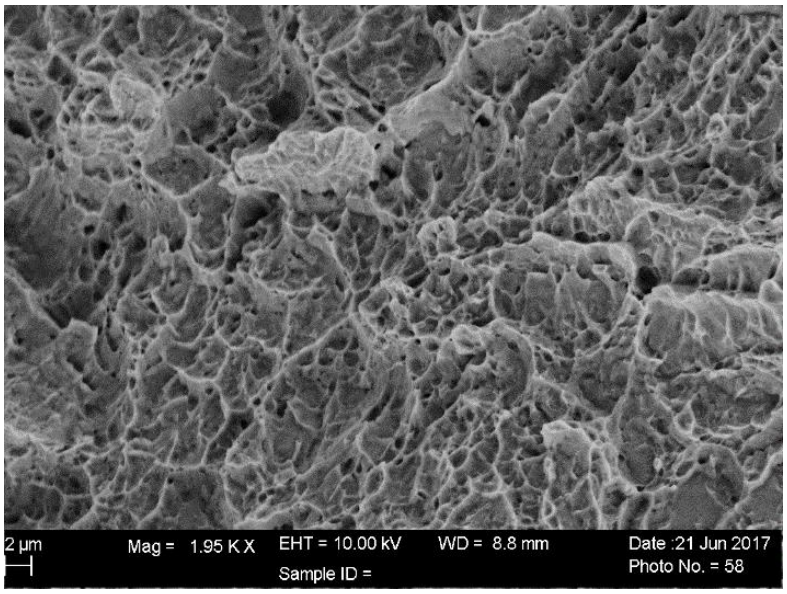

Figure 9: Dimple rupture surface for the third crack growth zone indicating ductile overload failure.

Discussion

It has been well established that increasing surface roughness is detrimental to the fatigue behavior of most materials [20]. Interestingly, this research has shown that, for additive manufactured parts in the as-built condition with high surface roughness, the effect is compounded by increasing surface area of a given part. The S-N curves presented in Figure 5 show the obvious trend of decreasing fatigue lives for increasing surface area, all of which maintained a similar gage volume size of 123 mm^3. The detrimental effect of increasing surface area is, in part, a result of increasing crack initiation sites. Figure 10 shows a representation of the crack initiation sites associated with each sample geometry for a stress amplitude of 200 MPa. While sample set #1 and #2 showed similar numbers of crack initiation sites, sample set #3 showed significantly more initiation sites and shorter lengths until cracks began the coalescence process. With increasing surface area, the likelihood that multiple crack initiation sites will occur near one another is increased leading directly to earlier crack coalescence and shorter fatigue lives.

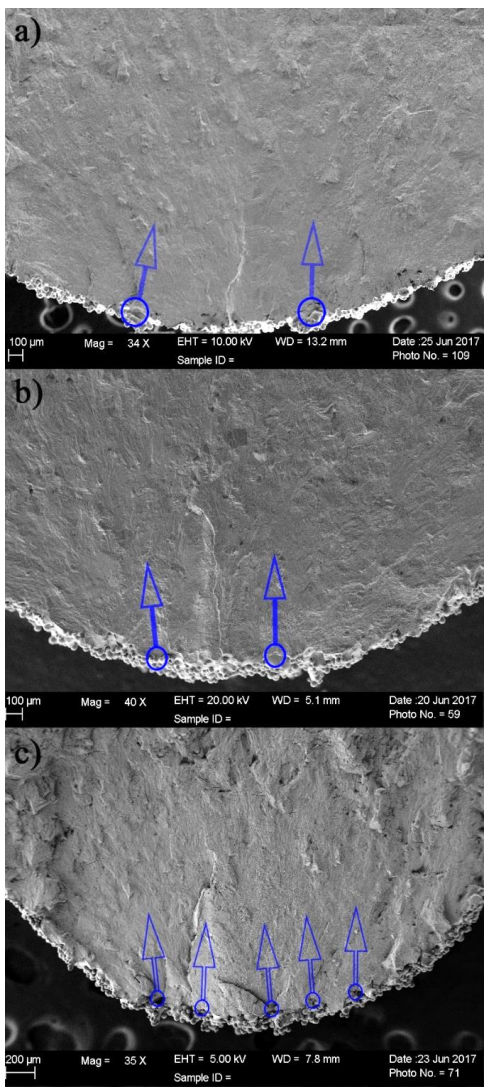

Figure 10: Crack initiation sites for a) sample set #1 b) sample set #2 and c) sample set #3.

Additionally, the first two crack growth zones were found to be a larger for the smaller surface area samples. This is shown in Figure 11 for samples #1 and #3 which had the smallest and largest surface areas respectively. This also appears to be a result of the increased likelihood of multiple cracks initiating near each other and crack coalescence occurring much earlier in the fatigue life. The stable crack growth zone (blue) in Figure 11 was determined to cover approximately 30% of the fracture surface for sample set #1 compared to just 16% for sample set #3. Additionally, the quasi-stable crack growth zone (red) in Figure 11 covers approximately 55% for sample set #1 and 40% for sample set #3. The final ductile overload zone (white) is also significantly more torturous for sample set #3.

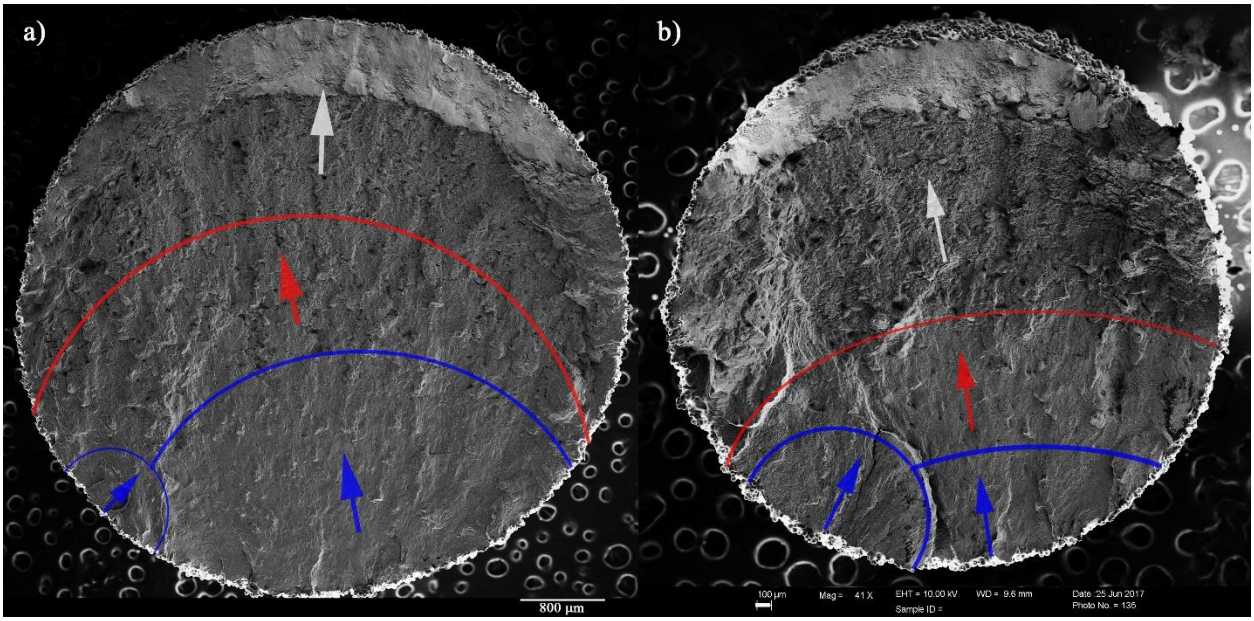

Figure 11: Crack growth zones for a) sample set #1 and b) sample set #3

Summary

Increasing surface area for a given volume size was found to be detrimental to the fatigue life of AM L-PBF produced Ti-6Al-4V parts. This is, in part, a result of the increased likelihood that multiple cracks will initiate in close proximity to each other. The fatigue crack growth zones for the increased surface area samples were found to be comparatively smaller than the samples with smaller surface areas. Additionally, the second crack growth zones were found to contain both static and cyclic failure modes which could explain why the fatigue endurance limit shows such a drastic reduction when compared to wrought Ti-6Al-4V alloys. These results indicate that geometry design for AM produced parts could improve the fatigue behavior for parts that will not undergo post-process machining by limiting the exposed as-built surface area.

Acknowledgement

This work was partially funded by the National Science Foundation under Grant No. 1657195. Support from the Naval Air Systems Command (NAVAIR) and Magee Technologies LLC is also greatly appreciated.

References

[1] C. N. Elias, J. H. C. Lima, R. Valiev, and M. A. Meyers, "Biomedical applications of titanium and its alloys," *JOM*, vol. 60, no. 3, pp. 46–49, Mar. 2008.

[2] M. Niinomi, "Recent metallic materials for biomedical applications," *Metall. Mater. Trans. A*, vol. 33, no. 3, p. 477, Mar. 2002.

[3] H. J. Rack and J. I. Qazi, "Titanium alloys for biomedical applications," *Mater. Sci. Eng. C*, vol. 26, no. 8, pp. 1269–1277, Sep. 2006.

[4] M. Niinomi, "Mechanical properties of biomedical titanium alloys," *Mater. Sci. Eng. A*, vol. 243, no. 1, pp. 231–236, Mar. 1998.

[5] B. L. Boyce and R. O. Ritchie, "Effect of load ratio and maximum stress intensity on the fatigue threshold in Ti–6Al–4V," *Eng. Fract. Mech.*, vol. 68, no. 2, pp. 129–147, Feb. 2001.

[6] R. K. Nalla, R. O. Ritchie, B. L. Boyce, J. P. Campbell, and J. O. Peters, "Influence of microstructure on high-cycle fatigue of Ti-6Al-4V: Bimodal vs. lamellar structures," *Metall. Mater. Trans. A*, vol. 33, no. 3, pp. 899–918, Mar. 2002.

[7] M. Niinomi, "Mechanical biocompatibilities of titanium alloys for biomedical applications," *J. Mech. Behav. Biomed. Mater.*, vol. 1, no. 1, pp. 30–42, Jan. 2008.

[8] R. K. Nalla, I. Altenberger, U. Noster, G. Y. Liu, B. Scholtes, and R. O. Ritchie, "On the influence of mechanical surface treatments—deep rolling and laser shock peening—on the fatigue behavior of Ti–6Al–4V at ambient and elevated temperatures," *Mater. Sci. Eng. A*, vol. 355, no. 1, pp. 216–230, Aug. 2003.

[9] H. Matsumoto *et al.*, "Room-temperature ductility of Ti–6Al–4V alloy with α′ martensite microstructure," *Mater. Sci. Eng. A*, vol. 528, no. 3, pp. 1512–1520, Jan. 2011.

[10] P. E. Carrion and N. Shamsaei, "Strain-based fatigue data for Ti–6Al–4V ELI under fully-reversed and mean strain loads," *Data Brief*, vol. 7, pp. 12–15, Jun. 2016.

[11] N. Shamsaei, A. Yadollahi, L. Bian, and S. M. Thompson, "An overview of Direct Laser Deposition for additive manufacturing; Part II: Mechanical behavior, process parameter optimization and control," *Addit. Manuf.*, vol. 8, pp. 12–35, Oct. 2015.

[12] A. J. Sterling, B. Torries, N. Shamsaei, S. M. Thompson, and D. W. Seely, "Fatigue behavior and failure mechanisms of direct laser deposited Ti–6Al–4V," *Mater. Sci. Eng. A*, vol. 655, pp. 100–112, Feb. 2016.

[13] P. Edwards and M. Ramulu, "Fatigue performance evaluation of selective laser melted Ti–6Al–4V," *Mater. Sci. Eng. A*, vol. 598, pp. 327–337, Mar. 2014.

[14] E. Wycisk, A. Solbach, S. Siddique, D. Herzog, F. Walther, and C. Emmelmann, “Effects of Defects in Laser Additive Manufactured Ti-6Al-4V on Fatigue Properties,” *Phys. Procedia*, vol. 56, pp. 371–378, Jan. 2014.

[15] H. Gong, K. Rafi, H. Gu, T. Starr, and B. Stucker, “Analysis of defect generation in Ti–6Al–4V parts made using powder bed fusion additive manufacturing processes,” *Addit. Manuf.*, vol. 1, pp. 87–98, Oct. 2014.

[16] A. Bauereiß, T. Scharowsky, and C. Körner, “Defect generation and propagation mechanism during additive manufacturing by selective beam melting,” *J. Mater. Process. Technol.*, vol. 214, no. 11, pp. 2522–2528, Nov. 2014.

[17] L. Thijs, F. Verhaeghe, T. Craeghs, J. V. Humbeeck, and J.-P. Kruth, “A study of the microstructural evolution during selective laser melting of Ti–6Al–4V,” *Acta Mater.*, vol. 58, no. 9, pp. 3303–3312, May 2010.

[18] L. E. Murr *et al.*, “Microstructures and mechanical properties of electron beam-rapid manufactured Ti–6Al–4V biomedical prototypes compared to wrought Ti–6Al–4V,” *Mater. Charact.*, vol. 60, no. 2, pp. 96–105, Feb. 2009.

[19] *ASM Handbook, Fatigue and fracture*, vol. 19. ASM International, 1996.

[20] R. I. Stephens, A. Fatemi, R. R. Stephens, and H. O. Fuchs, *Metal Fatigue in Engineering*. John Wiley & Sons, 2000.